Meteoritics & Planetary Science 41, Nr 10, 1469–1482 (2006)
Abstract available online at http://meteoritics.org

Morphology and geometry of the distal ramparts of Martian impact craters

Peter J. MOUGINIS-MARK[1*] and Stephen M. BALOGA[2]

[1]Hawai'i Institute of Geophysics and Planetology, University of Hawai'i, Honolulu, Hawai'i 96822, USA
[2]Proxemy Research, Inc. Laytonsville, Maryland, USA
[*]Corresponding author. E-mail: pmm@higp.hawaii.edu

(Received 12 October 2005; revision accepted 20 May 2006)

Abstract–We used Mars Orbiter Laser Altimeter (MOLA), Thermal Emission Imaging System visible light (THEMIS VIS), and Mars Orbiter Camera (MOC) data to identify and characterize the morphology and geometry of the distal ramparts surrounding Martian craters. Such information is valuable for investigating the ejecta emplacement process, as well as searching for spatial variations in ejecta characteristics that may be due to target material properties and/or latitude, altitude, or temporal variations in the climate. We find no systematic trend in rampart height that would indicate regional variations in target properties for 54 ramparts at 37 different craters 5.7–35.9 km in diameter between 52.3°S to 47.6°N. Rampart heights for multi-lobe and single-lobe ejecta are each normally distributed with a common standard deviation, but statistically distinct mean values. Ramparts range in height from 20–180 m, are not symmetric, are typically steeper on their distal sides, and may be as much as ~4 km wide. The ejecta blanket proximal to parent crater from the rampart may be very thin (<5 m). A detailed analysis of two craters, Toconao crater (21°S, 285°E) (28 measurements), and an unnamed crater within Chryse Planitia (28.4°N, 319.6°E) (20 measurements), reveals that ejecta runout distance increases with an increase in height between the crater rim and the rampart, but that rampart height is not correlated with ejecta runout distance or the thickness of the ejecta blanket.

INTRODUCTION

The emplacement mechanism of the fluidized ejecta around impact craters on Mars has been a controversial topic almost since the discovery of these craters in Viking Orbiter images. The term "fluidized" has been applied to these ejecta not necessarily because they possessed water at the time of emplacement, but rather because there is strong geomorphic evidence that shows that the ejecta flowed across the surface. Different opinions still exist about the emplacement of ejecta associated with the three main types of impact crater on Mars, namely, single-layer ejecta (SLE), double-layer ejecta (DLE) and multiple-layer ejecta (MLE), as defined by Barlow et al. (2000). The interpretation that volatiles are responsible for the fluid flow of the ejecta has relied primarily on the fluid appearance of the ejecta (Carr et al. 1977; Gault and Greeley 1978; Mouginis-Mark 1979) and the evidence for similar fluidized ejecta on icy satellites (Horner and Greeley 1982; Moore et al. 2001). The alternative idea—that fluid flow of the ejecta was due to strong winds generated by impact— comes from the similarity in appearance between fluidized crater ejecta seen on Mars and flow generated in the presence of an atmosphere in the laboratory (Schultz and Gault 1979, 1982; Schultz 1992). The possibility that fluidized ejecta are the result of dry granular flows that do not require any fluidizing agent is also a possibility (Barnouin-Jha 2005; Barnouin-Jha et al. 2005).

Despite the potential significance that the morphology of the ejecta layers holds for providing information on the dynamics of cratering process, few detailed studies of the deposits have been made. Barlow (2004) has studied the ejecta mobility (EM) ratio, which is the ratio of the ejecta extent to the crater radius, and this is believed to provide information about the fluidity of the ejecta during emplacement. Variations in the EM ratio occur within each ejecta morphology type and with location, suggesting that volatile concentrations were spatially variable at the time of crater formation (Mouginis-Mark 1979, 1981; Costard 1989). However, Barlow (2004) inferred from both regional and local analyses of crater ejecta morphology that concentrations of subsurface volatiles have remained approximately constant at the depths and over the time periods recorded by the craters. In an early experimental study of rampart crater formation, Wohletz and Sheridan

(1983) proposed that ramparts are deposited as a result of the transition from quasi-fluidized viscous ejecta to inertial fixed-bed emplacement. They suggested that the movement of initially viscous ejecta decreased in energy and degree of fluidization as the material moved away from the parent crater. At the distance from the crater where the flows dropped below the critical fluidizing level, deposition of ramparts took place en masse as the shear stress of the flow decreased below the yield strength. Barnouin-Jha et al. (2005) investigated the similarities and differences between rampart crater emplacement and terrestrial and Mars landslides. Their analysis considered factors such as runout distance, deposit topography, the presence of boulders in the distal deposits. They also used a kinematic model based on the conservation of flow volume that highlighted the similarity of continuum ejecta flow to landslide emplacement when the differences in emplacement geometry were accounted for.

Baloga et al. (2005) constructed a basic continuum flow model for the emplacement of the distal rampart deposits on Mars. This model extends the approach used in Barnouin-Jha et al. (2005) by postulating an independent description of momentum conservation during transit. They found that three factors led to the formation of sharp distal peaks. First, there must be sufficient material ejected so that the transport resembles a continuum fluid flow. Second, there must be some form of local resistance to flow that dissipates the momentum along the flow path. Third, the basic processes of flow momentum and volume conservation, in cylindrical geometry, combined with elementary boundary conditions at the source, naturally produce flow thickness profiles with sharp frontal peaks (i.e., distal ramparts). Moreover, this behavior is essentially independent of the form of the flow depth boundary condition.

To date, none of the investigations have focused on the detailed structure or topographic signature of the ejecta deposits, despite the potential information that they provide with respect to the mode of formation (Mouginis-Mark 1981), the source of fluidization (Ivanov 1996; Barnouin-Jha and Schultz 1998), and the rheology (Baratoux et al. 2002) of the ejecta deposits. With the availability of image data from the Mars Orbiter Camera (MOC) and the Thermal Emission Imaging System (THEMIS), as well as detailed topographic data from the Mars Orbiter Laser Altimeter (MOLA), it is now possible to investigate these properties. Using selected examples of fresh impact craters on Mars where the distribution of these data sets permits measurement of the ejecta deposits, we document the thickness, shape, and spatial variation of the distal ramparts around 37 craters 5.7–35.9 km in diameter. We also conduct a more detailed investigation of ejecta runout distance, rampart height, and the "fall-height" of the ejecta from the parent crater rim using the crater Toconao, which is located in Sinai Planum and an unnamed crater within Chryse Planitia.

MORPHOLOGY OF THE DISTAL RAMPARTS

In this investigation we use only the freshest appearing impact craters so that the ramparts included here are the most likely to have the least amount of erosion. The most obvious characteristic of Martian SLE and MLE craters is the distal ridge or "rampart" that surrounds the perimeter of the ejecta layer. Indeed it was this attribute that originally prompted the term "rampart crater" (Carr et al. 1977). These ramparts are often quite sinuous (Barlow 1994). The distal boundary of the outer ejecta layer of DLE craters is different from the rampart of the SLE and MLE craters (Boyce and Mouginis-Mark 2006); there is no prominent rampart associated with the edge of the outer ejecta layer of DLE craters. Instead, there is a convex-upward edge to the ejecta, and MOLA data show that the change in height from the surface of the ejecta to the surrounding terrain is of the order of only a few meters. The results presented here do not, therefore, pertain to the geometry of the distal deposits of DLE craters.

Early inferences about the mode of formation of the distal ramparts of SLE and MLE craters (Carr et al. 1977; Wohletz and Sheridan 1983) were that they are deceleration ridges, akin to the distal rampart observed on certain terrestrial landslides such as the Blackhawk slide in California, USA (Shreve 1968). Viking and THEMIS (Fig. 1) data show that this rampart has several distinct attributes, the most obvious of which is that the distal ridge is typically continuous around the entire perimeter of the ejecta layer. Baratoux et al. (2005) have shown from THEMIS IR data of Syrtis Major that there is a systematic relative increase in temperature at night of the ramparts, which is most likely associated with an increase in the particle sizes of materials within the rampart relative to the rest of the ejecta blanket, perhaps by some kinetic sieving process during emplacement. Closer inspection of the ramparts using THEMIS VIS and MOC images (Fig. 2) further demonstrates that the ramparts may have been emplaced as "pulsed flows" wherein one lobe of ejecta was followed by a second or third lobe (Fig. 2a), that some ejecta lobes not only possess distal ramparts but also side-ridges that are radial to the direction of ejecta flow (Fig. 2b), that radial striations may extend onto the rampart (Fig. 2c), and that some ramparts have large blocks or boulders preserved on the rampart crest (Fig. 2d) consistent with the increase in particle size proposed by Baratoux et al. (2005). Ejecta layers appear to have been emplaced essentially as solitary sheets of material that can be traced from the distal ramparts approximately to the crater rim. The simplest choice for an emplacement mechanism suggested by the examples we have examined is one of a continuous flow that moved across the preexisting surface from a point near the rim out to the distal locations observed today. Although there may be a few anomalies, the material comprising the distal ramparts generally issued from close to the crater rim before the proximal deposit constituents that now reside beside it.

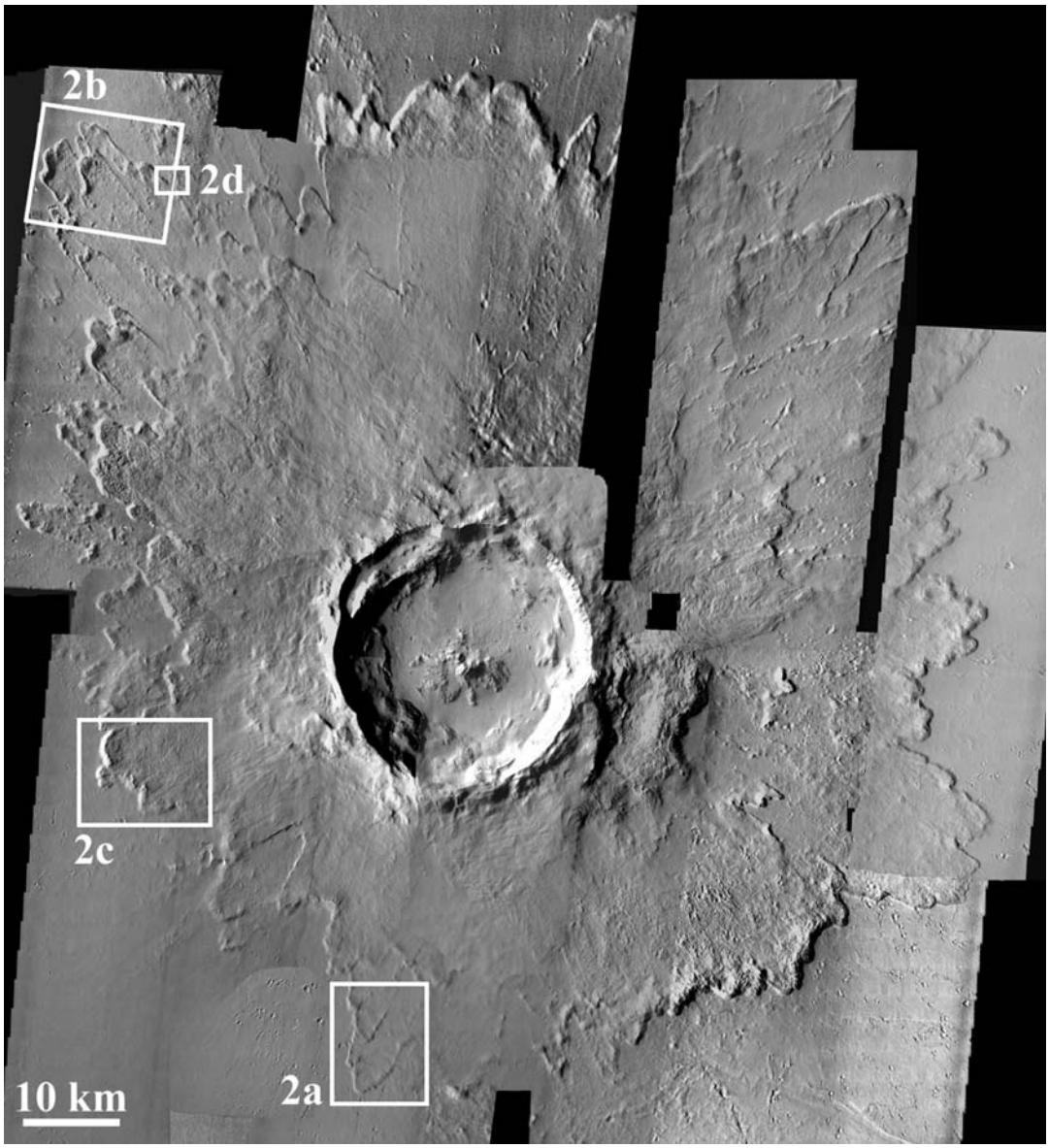

Fig. 1. Tooting crater, a 29 km-diameter crater located to the west of the Olympus Mons aureole at 23.2°N, 207.8°E. Rectangles indicate the locations of Fig. 2. Mosaic of THEMIS VIS images V01965003, V01990003, V05011006, V05710012, V09879009, V10528009, V10815008, V10840007, V11152006, V11439007, V11464014, V12063004, V12350008, V12662009, V13286006, V13573002, V135980098, and V14197013.

To further define the cross-sectional shape of the ramparts, we have used photoclinometry (a frequently used technique that provides shape from shading; Davis and Soderblom 1984), coupled with MOLA elevation data, to determine the cross-sectional shape of some ramparts (Fig. 3). We have developed a technique (Garbeil and Mouginis-Mark, unpublished analysis) that allows pixel brightness values in calibrated THEMIS VIS images to be interpreted as slope variations facing towards or away from the Sun, provided that the albedo of the surface can be assumed constant (which is a reasonable assumption provided the length of the profile is only 2–4 km in length). Absolute height variations are controlled by MOLA point measurements at the start and end of the profile. The elevation change along the profile is also controlled by using the highest MOLA elevation measurement at the visually determined crest of the rampart. Raw MOLA precision engineering data record (PEDR) elevations are used for this elevation control. Using this technique, we find that ramparts can be as much as 1,700 m wide, and our photoclinometric measurements show that they can be as much ~150 m high. In cross-section, the ridge is found to be non-symmetric with the outer margin steeper than the inner margin. Looking in the direction of the parent crater, the ejecta layer is at a markedly lower elevation than the

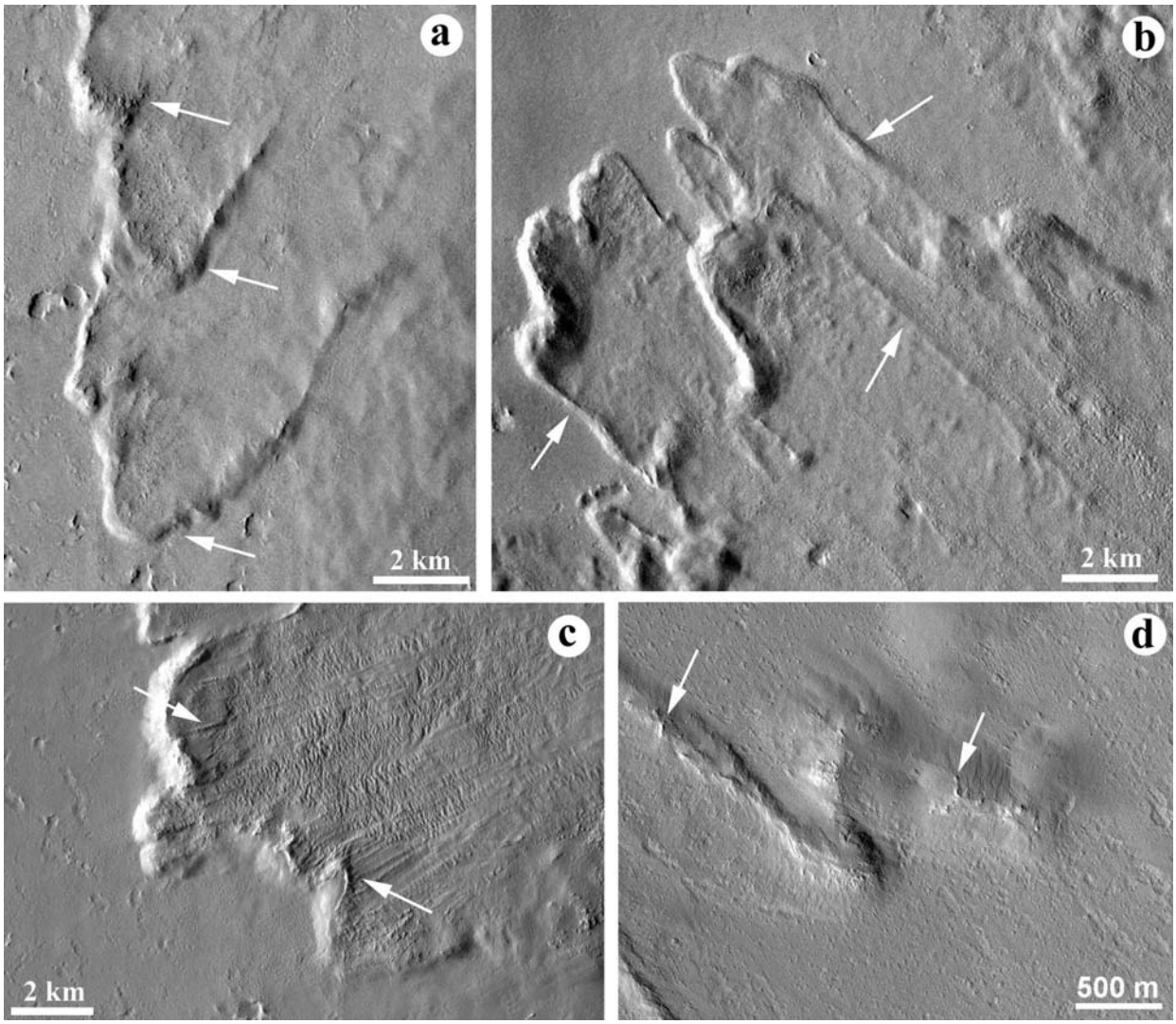

Fig. 2. Subscenes of THEMIS VIS and MOC images illustrating physical characteristics of the ejecta blanket of Tooting crater. See Fig. 1 for image locations. a) Multiple ejecta lobes (arrowed) showing that the rampart formed as surges of material rather than as a single flow event. Direction of flow is towards the lower left. THEMIS image V01990003. b) Several of the ejecta lobes have ramparts along the sides of the lobes (arrowed) in addition to the distal ramparts. Direction of flow towards the top left. THEMIS image V11152006. c) Radial striations extend on to the distal rampart (arrowed). Direction of flow towards lower left. THEMIS image V13598009. d) Boulders (arrowed), which could also be massive erosional remnants, appear to be concentrated at the crest of the distal rampart. Direction of flow is towards the top left. MOC image S0301050.

ridge. Such proportions are different from the model proposed by Wohletz and Sheridan (1983), who proposed that the rampart was constructed from a gradually thickening planar deposit.

There is often structure within the rampart, with crenulations parallel to the perimeter of the ejecta layer the most common attribute (Fig. 2c). Also evident from Fig. 3 is the surprising fact that the thickness of the ejecta blanket proximal to the parent crater (with respect to the rampart) is very thin. Assuming that the ejecta were not flowing up an inclined surface, then the ejecta blanket proximal to the crater from the rampart is often only a few (<10) meters thick.

DISTRIBUTION OF EJECTA GEOMETRY

Ideally, to fully investigate the geometric variability of the ejecta deposits, a global study of the heights of the ramparts, as well as the ejecta runout distances from the parent craters, should be conducted. Unfortunately, given the spatial distribution of the THEMIS VIS images collected to date, and the quality of the atmosphere at certain latitudes and times of year, such a “global” study is not possible at this time. Individual fresh craters are often the targets of VIS images of the northern plains, but only less frequently are craters the prime target in the southern hemisphere. In

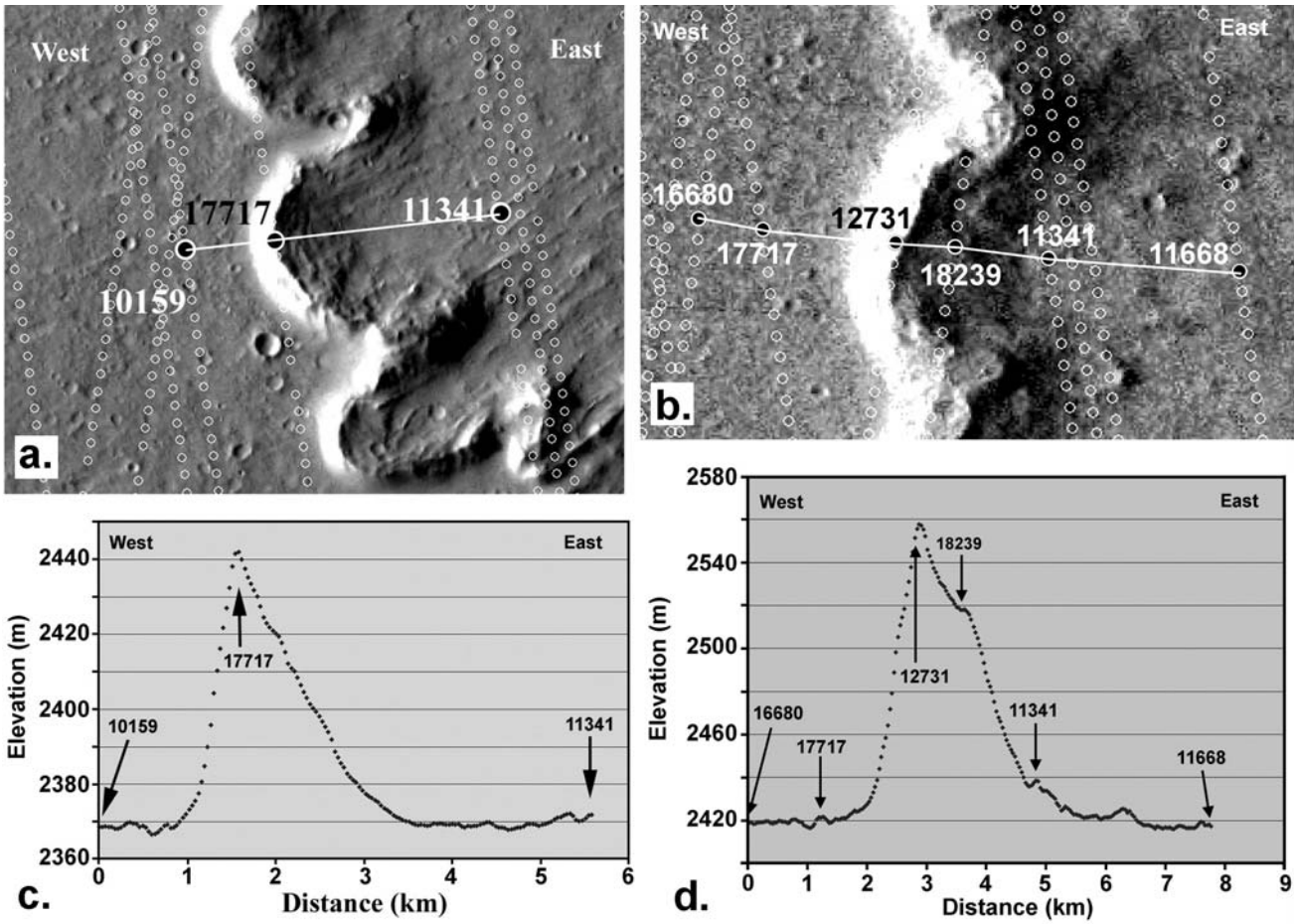

Fig. 3. Photoclinometric profiles across ejecta ramparts from Toconao crater, located in Sinai Planitia at 21°S, 285°E. a) and b) Location of MOLA profiles (open circles) and the photoclinometric profile across the rampart. In (a), the starting point on MOLA orbit 10159, the ending point on orbit 11341, and the elevation control on orbit 17717 are shown. In (b), the MOLA starting point on orbit 16680, the ending point on orbit 11668, and the elevation control on orbits 17717, 12731, 18239, and 11341. Base image for both profiles is THEMIS image V05808002. Bottom pair of images: Photoclinometrically derived topographic profiles derived from THEMIS image V05808002. The profile at left shows that the rampart is ~75 m high and ~2 km wide, and the profile at right demonstrates that the rampart is ~140 m high and ~3.5 km wide.

addition, we have inspected several hundred THEMIS VIS images of rampart craters, only to discover that the precise location of each MOLA ground track does not permit the height of the rampart to be determined. Thus, although our data set extends from 52.3°S to 47.6°N, most of the craters are found on plains materials. Only very rarely is it possible to find well preserved ramparts on craters located within the southern highlands; we leave to a future investigation an interpretation of this distribution, which is potentially related to the lack of mechanical strength of the highlands rocks and thus their inability to preserve the detailed morphology of the craters.

The radial extent of the ejecta flow, and the height of the distal rampart, may both be related to the degree of fluidization of the ejecta. Thus, we have explored the possibility that rampart heights may vary systematically across the planet, either as a function of crater size, or the latitude or elevation of the parent crater. Such trends have already been proposed for the different types of craters (Mouginis-Mark 1979; Horner and Greeley 1987; Barlow and Perez 2003), and may indicate that a thicker volatile layer is located at the higher latitudes.

Using a combination of MOLA PEDR data co-registered to THEMIS VIS images, we have been able to measure the heights of 54 ramparts associated with 37 different craters that are 5.0–35.9 km in diameter between 52.3°S to 47.6°N. (Fig. 4). All of these craters have well-preserved rims and ejecta blankets, so that we infer that these are some of the youngest large impact craters on Mars. Included in our sample are 9 SLE craters (as defined by Barlow et al. 2000) that are 9.5–15.8 km in diameter, and 28 MLE craters that are 5.7–35.9 km in diameter. For both types of craters, in order to make these measurements, we required that MOLA shots be available for the crest of the rampart, the terrain beyond the rampart (and within ~2 km of the foot of the rampart) and the ejecta blanket just upslope (by less than ~2 km) from the

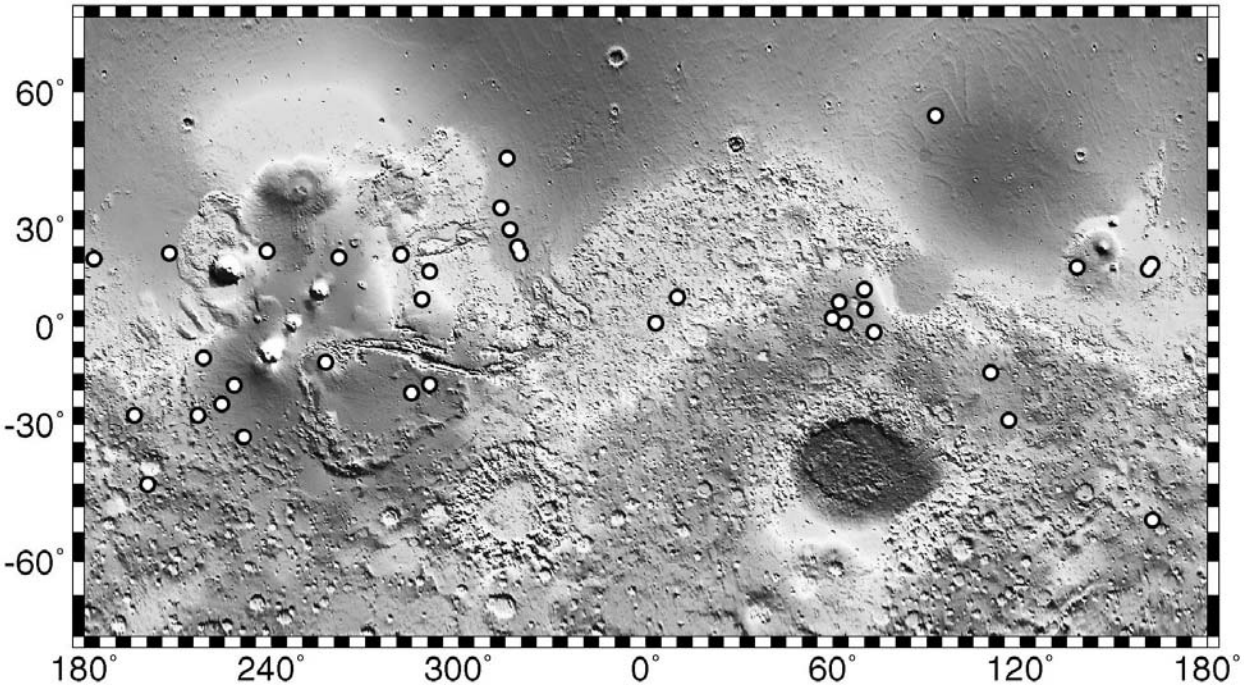

Fig. 4. Global distribution of 37 different craters with ramparts measured in this investigation. The number of craters that can be measured is limited by the coverage of the acquired THEMIS VIS images, the distribution of MOLA profiles across the distal ramparts, and the constraint that only the clearest examples of ramparts were measured.

rampart. The MOLA PEDR data were projected on to THEMIS VIS images (at 18 m/pixel resolution) so that the detailed morphology of the rampart could also be identified to ensure correct placement of the MOLA elevation measurements. These criteria precluded our analysis of many potential SLE and MLE craters for two reasons: (a) the crater had not been imaged by THEMIS, and (b) the distribution of MOLA shots was such that at least one of the three required elevations (rampart crest and both sides of the foot of the rampart) could not be measured.

Our results for the 54 ramparts are shown in Fig. 5, which illustrates (a) the mobility of the ejecta normalized to parent crater size (i.e., the ejecta mobility ratio of Mouginis-Mark 1978) against crater latitude; (b) the height of the ejecta rampart versus the latitude of the parent crater; and (c) the rampart height versus the elevation of the parent crater. Craters are subdivided into SLE and MLE craters. Evident from these three plots is the apparent lack of correlation for ejecta morphology between either ejecta mobility or the height of the distal rampart when compared to the crater latitude or elevation. There is an increase in average ejecta mobility at higher northern latitudes (Fig. 5a), and for these same craters the rampart height is much less than at other latitudes (Fig. 5b). Generally, the ramparts show the same range in heights (from 50–150 m) in both hemispheres, although all of the smallest ramparts (25–45 m high) are in the northern hemisphere. There is also a lack of correlation between rampart height and the elevation of the crater (which ranges from +4,000 to –5,000 m relative to the MOLA datum), with the possible exception that several of the highest ramparts (>130 m) are found at elevations higher than 2 km above the datum.

Baloga et al. (2005) inferred that the speed of ejecta emplacement was quite slow (of the order of 25–115 m/s) compared to expectations based on ballistic-dominated transport. They proposed that as the flow progressed away from the crater rim, the flow front rapidly slowed and formed a sharp peak. Our observation that the proximal and distal sides of the rampart are at very similar elevations also implies that the deceleration was rapid, as almost all of the material is concentrated in a narrow rampart rather than being spread out over an extended radial range. Clearly, however, our data set is quite limited due to the scattered distribution of THEMIS observations and MOLA topographic measurements. Additional measurements such as the ones presented in Fig. 5 need to be obtained from still-to-be-collected THEMIS images in order to determine if this lack of variability in rampart height persists. If there is no correlation, this most likely implies something fundamental about the mechanism by which the fluidized ejecta layers come to a stop, and should be further investigated as additional THEMIS images become available.

Statistical analysis of the rampart heights indicates that both the MLE and SLE craters have normal distributions with means of 74.54 m and 102.93 m, respectively, and standard deviations of 30.87 m (MLE) and 34.78 m (SLE). The standardized skewness and kurtosis were used as measures of the consistency of the rampart heights with the normal

distribution. When these standardized statistics lie within plus and minus 2, the distribution is considered to be consistent with the normal distribution. The standardized skewness and kurtosis are 1.31 and 0.04 for the MLE craters and 0.76 and −0.14 for the SLE craters.

The mean values of the distributions are significantly different according to a t-test assuming equal variances. The 95% confidence interval for the difference in the means extends from −47.89 to −8.90, so it is unlikely that the differences could come from a single population by chance. We have gone a step further by statistically testing the underlying assumption of this test, namely, the two populations have the same standard deviations. The standard F-test on the ratio of the variance gives a critical region from 0.29 to 1.76. Because this region contains 1, the variances of the MLE and SLE populations are considered statistically indistinguishable. This result supports the validity of the t-test conclusion.

The inference of a normal distribution suggests that rampart height is determined by a process or processes that produces a single mean value for rampart height for each population, regardless of crater diameter, location, or elevation within the population. The host of plausible factors governing rampart height, including variations in topography, lithology, and composition of the impactor or target, simply contribute modest random variations that combine to produce a normally distributed dispersion about the mean value. What is most interesting, however, is that the morphologic complexity of the deposits manifests as a shift in the mean between the MLE and SLE populations.

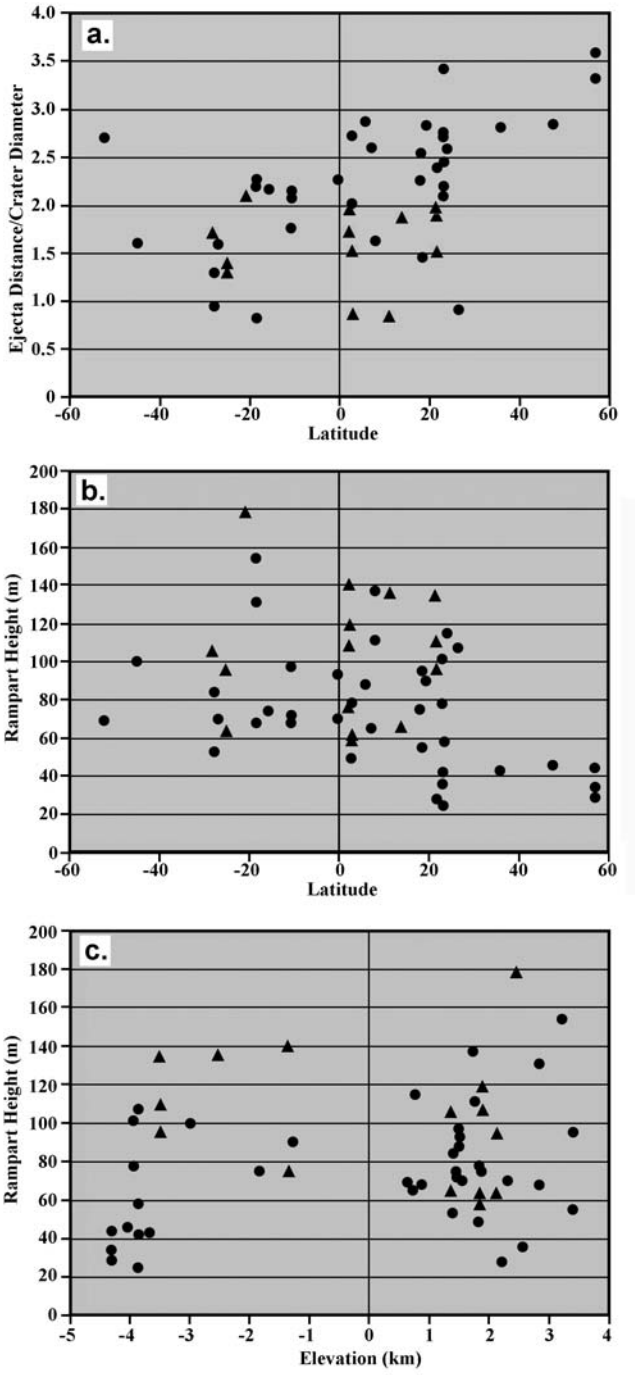

Fig. 5. Distribution of 54 rampart heights and ejecta runout distances for the 37 different craters shown in Fig. 4. a) Ejecta range normalized to the diameter of the parent crater compared to the latitude of the crater. b) Rampart heights as a function of latitude. c) Rampart heights as a function of target elevation. These data show that there is no strong correlation between the parameters, suggesting that rampart formation is not a function of local environmental conditions.

RAMPARTS AT INDIVIDUAL CRATERS

Toconao Crater

A 17.9 km-diameter crater in Sinai Planum (at 21°S, 285°E), named Toconao (after a small town in the Atacama Desert of northeast Chile), provides an opportunity to make detailed measurements of the geometry of an ejecta blanket and the parent crater. A single continuous distal rampart extends around the Toconao crater, and is particularly clearly defined on the western side (Fig. 6). It is possible to measure several attributes of the ejecta blanket of the Toconao crater using the combined MOLA PEDR and THEMIS data sets (Fig. 7). As is illustrated in Fig. 8, these attributes include (a) the elevation of the rim crest; (b) the elevation of the top of the collar of ejecta surrounding the parent crater; (c) the elevation of the base of the ejecta collar; (d) the radial distance between the rim crest and the proximal base of the rampart; (e) the elevation of both the proximal and distal base of the rampart; and (f) the elevation of the crest of the rampart. From these measurements, the height of the rampart above the surrounding terrain, the drop in height of the ejecta from the top of the collar to the base of the rampart, the thickness of the ejecta blanket proximal to the crater from the rampart, and the width of the rampart can all be calculated.

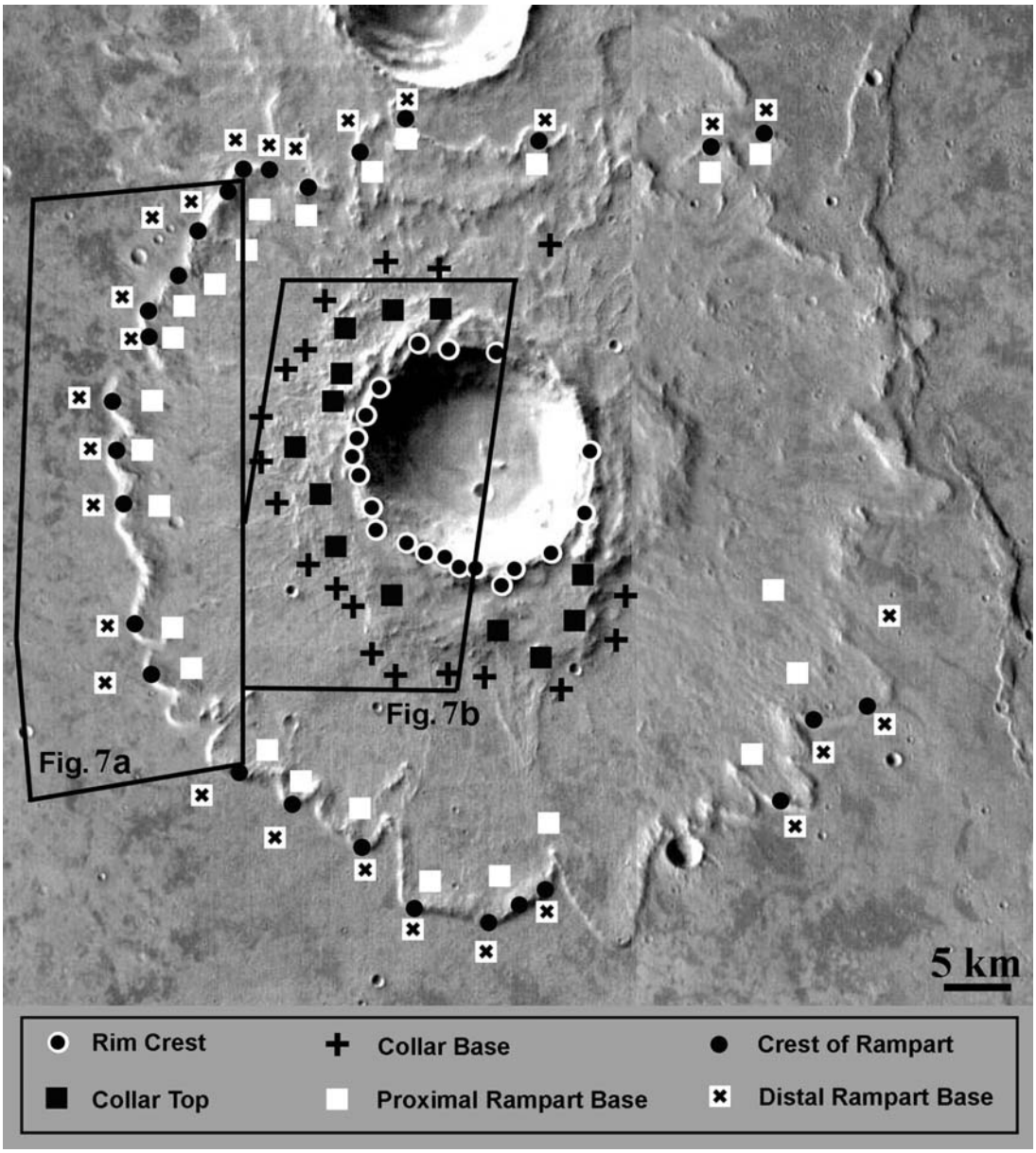

Fig. 6. Toconao crater, located in Sinai Planum at 21°S, 285°E, showing the locations of detailed segments illustrated in Fig. 7. THEMIS images I05059003 and I06894002.

In Fig. 9, we investigate three possible geomorphic relationships for the ejecta blanket. First, we explore the possibility that individual ejecta lobes traveled a radial distance that is proportional to the change in elevation from the top of the ejecta collar to the base of the rampart. Such a correlation might be expected if the ejecta lobes are analogous to large landslides (Barnouin-Jha et al. 2005). Based on the distribution of MOLA shots that are located at the base of the ejecta collar and the proximal base of the rampart, we were able to collect elevation information for 28 different azimuths from the center of Toconao crater. Evident from Fig. 9a is a slight indication that the ejecta flowed to a greater radial distance when the height drop from the top of the collar to the foot of the rampart is greater. Interestingly, there is a large variation in runout distance for the same drop in height from the collar; for example, a drop of ~80 m may produce a runout distance of ~15 km to 27 km. Similarly, comparable runout distances may be associated with strikingly different drops in elevation from the collar top; for example a runout distance of ~25 km was produced for drops in height from the collar of ~85–195 m. Given the shape of the crater rim, it is unlikely that the trend in rampart runout distance could be attributed to an oblique impact. However, this possibility cannot be rigorously precluded and similar analyses of other rampart crater deposits are warranted.

We can also measure the height and width of 28 different

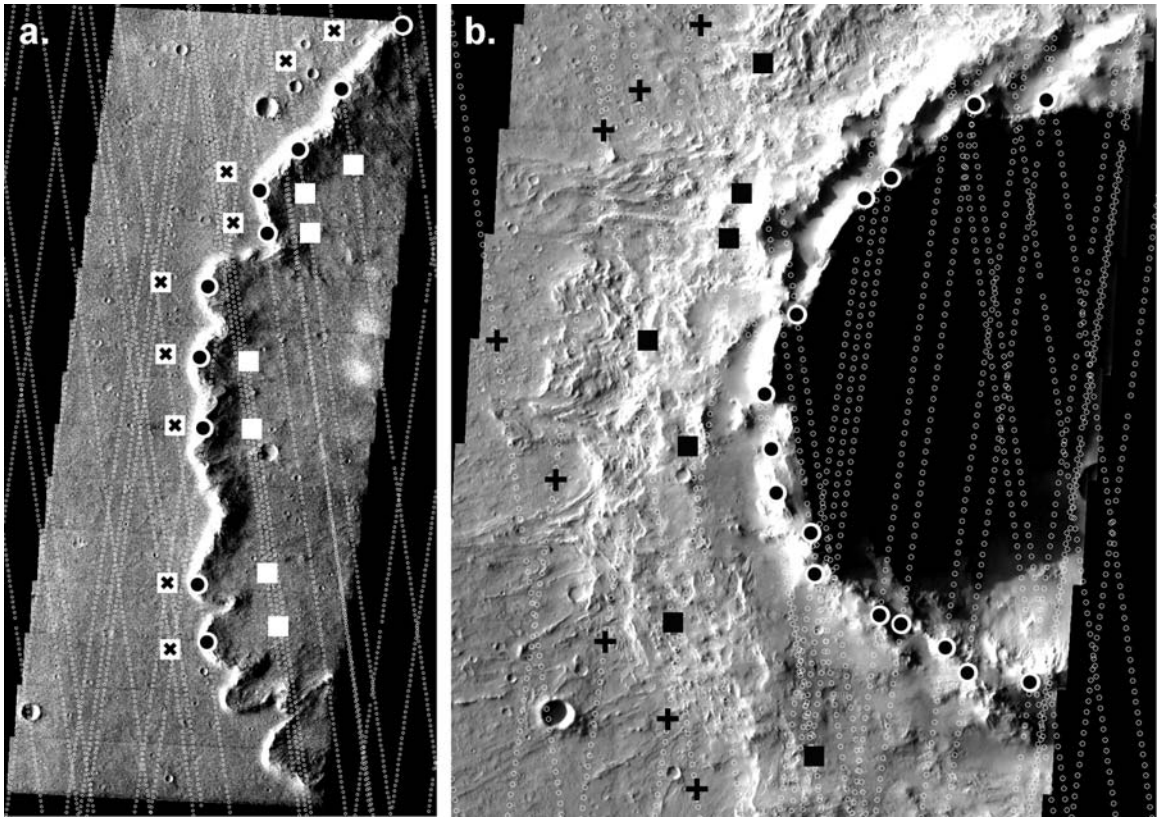

Fig. 7. Distribution of MOLA ground tracks for Toconao crater, also showing the locations where elevation data were collected in this analysis. See Fig. 6 for locations. a) The western ejecta blanket. Circles show the places where the elevations were measured proximal and beyond the rampart, and the squares mark the places where elevations were measured on the crest of the rampart. THEMIS image V05808002. b) The crater rim crest (squares) and the base of the ejecta collar (circles). THEMIS image V11200004.

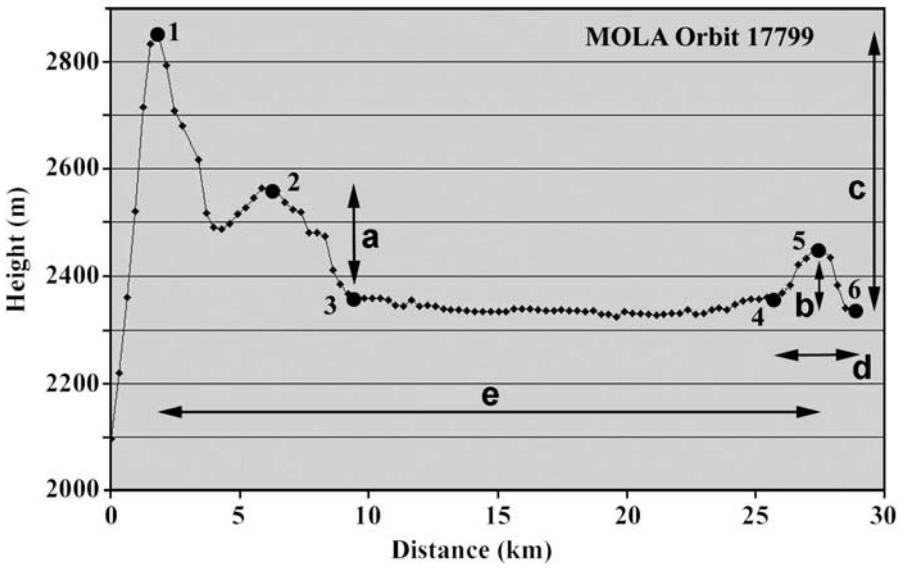

Fig. 8. Schematic of the parameters measured for the ejecta blanket of Toconao crater. Base profile is from MOLA orbit 17799. (1) Rim crest. (2) Top of ejecta collar. (3) Base of ejecta collar. (4) Base of rampart on crater-facing side. (5) Crest of rampart. (6) Base of rampart away from crater; “a” drop in height between the top and base of the collar; “b” height of rampart; “c” fall height from crater rim crest to distal base of rampart; “d” width of rampart; and “e” ejecta runout distance from crater rim crest to crest of rampart.

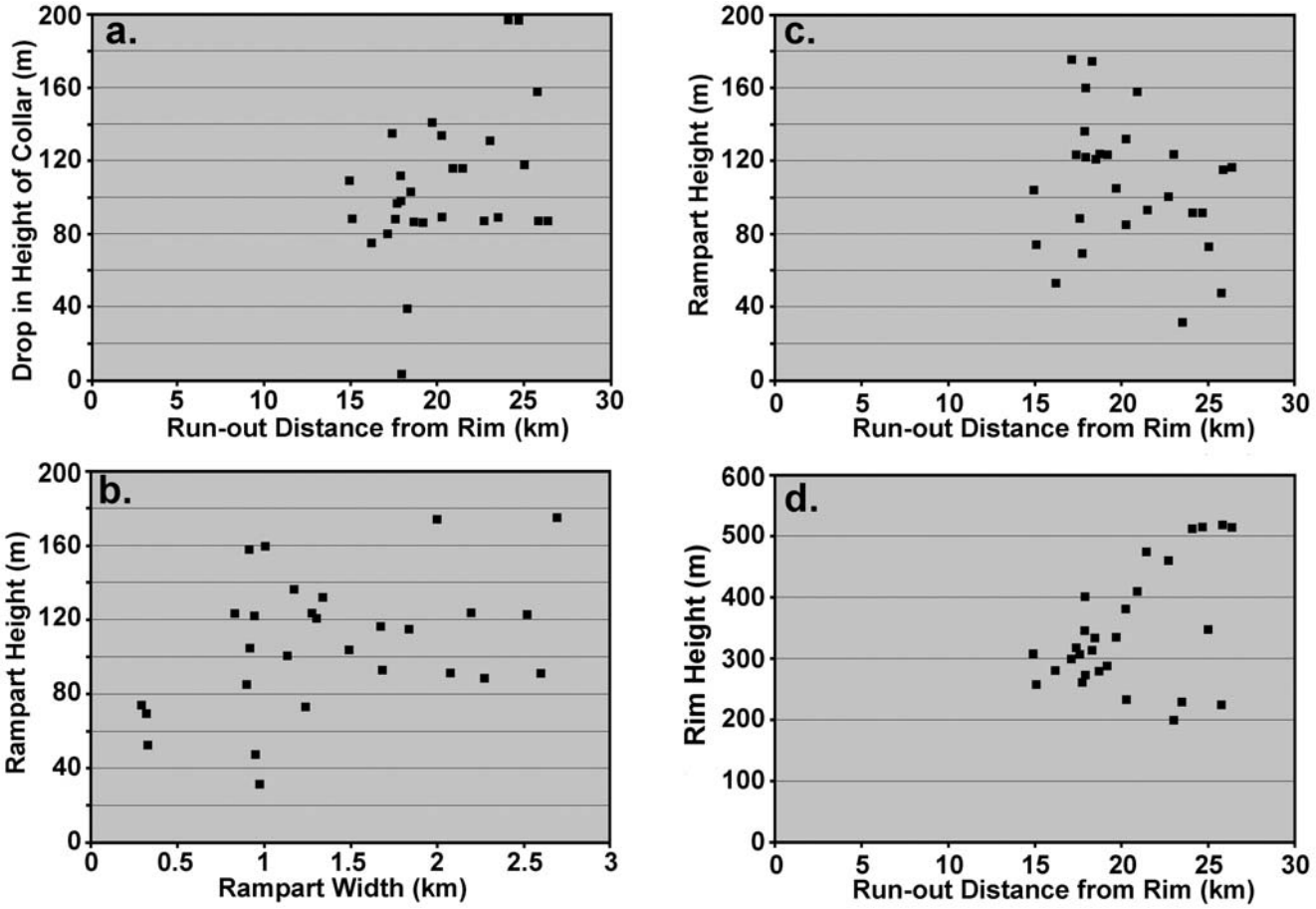

Fig. 9. Geometry of ramparts at Toconao crater. See Fig. 8 for locations where ramparts were measured. a) Runout distance of the ejecta lobe as a function of the drop in height from the base of the ejecta collar ("a" in Fig. 8) to the distance traveled from the crater rim ("e," Fig. 8). b) Rampart height ("b") compared to the width of the rampart ("d"). c) Rampart height ("b") compared to the runout distance from the crater rim ("e"). d) Rim height ("c") compared to runout distance from the crater rim ("e").

ramparts around Toconao crater (Fig. 9b). Such information allows the height of the rampart to be compared to rampart width, thus providing a diagnostic of the rate of flow momentum distribution (Baloga et al. 2005). The volume of material contained within the rampart can also be compared to the entire ejecta blanket. Our data show considerable variability in the dimensions of the rampart. The smallest ramparts have heights of ~50–70 m and are ~300 m wide (i.e., base-to-height ratio of 6:1 to 4.25:1), while the largest rampart is ~170 m high and ~2,700 m wide (base-to-height ratio of almost 16:1). However, some of the highest ramparts observed are not the widest, but are ~160 m high and ~1,000 m wide (base-to-height ratio of 6.25:1).

We have also explored the possible relationship between the height of the rampart and the distance that the ejecta traveled from the crater rim (Fig. 9c). In particular, we have searched for a correlation wherein rampart height was consistently less as the travel distance increased. Such a correlation might exist if an azimuthally uniform volume of ejecta was produced and the ejecta blanket had a significant thickness, thereby using the majority of the volume to make the ejecta blanket and progressively "starve" the ramparts of material as the runout distance increased. Although there are many ramparts that are smaller than the maximum at a given distance, this trend is only partially suggested by our measurements. The highest ramparts (~175 m) are found at a radial distance of ~20 km from the rim, and the maximum height decrease as one goes further from Toconao so that at a radial distance of ~27 km the maximum height is ~115 m (i.e., 60 m lower). Some of the lowest ramparts are also found closest to the parent crater (at ~16 km from the rim), albeit on the northern part of the blanket (which is the up-slope direction from the Toconao crater). The two lowest ramparts (<50 m high) are found at a distance of ~23–27 km. A formal test for correlation between the rampart height and runout distance by the Pearson Product Moment (PPM) coefficient indicates no significant correlation.

Figure 9d explores the potential correlation between the rim height of Toconao (as measured relative to the base of the rampart) and the runout distance for the ejecta layer. Here there is an apparent increase in the runout distance with increasing rim height. The PPM coefficient (e.g., Sheskin

1997) indicates a modest relationship exists between these variables. For a drop of 300 m from the rim crest, the rampart is ~15 km away. A drop in height of 500 m may allow the ejecta to travel ~25 km from the rim. While it is tempting to say that this is a true correlation, which would have implications for a gravity-driven origin for the ejecta flows, we caution the reader that the measurement of the crater rim height (and thus the drop in height to the rampart) is extremely difficult to measure with confidence. In places where the topography is steepest, the finite size of the MOLA footprint and the precise location of the spot on the rim crest may give inaccurate values for the elevation of the rim. Moreover, the statistical test for correlation between rim height and runout distance by the PPM coefficient is significantly influenced (Sheskin 1997) by the small group of data points at the extreme upper limit of rim height. Nevertheless, the apparent correlation displayed in Fig. 9d is tantalizing, and warrants the collection of additional data at such time that higher resolution topographic data permit the true height of the rim crest to be determined.

Chryse Crater

The data presented in Fig. 9 for Toconao, while they may provide insights into the ejecta emplacement process, may not be application for all MLE craters on Mars. At this time, it is extremely difficult to identify individual craters for which more than half a dozen rampart heights can be measured. As mentioned above, this is partially due to the spatial distribution of the THEMIS VIS images that have to date been obtained, and partially due to the precise locations of the MOLA groundtracks with respect to the ramparts. To explore the potential unique quality of the Toconao data, we have been able to produce a similar data set for an unnamed 16.0 km in diameter crater in Chryse Planitia (at 28.4°N, 319.6°E). This crater is at an elevation of −3.9 km relative to the Mars datum, making a difference of >6.6 km compared to Toconao. The distribution of MOLA PEDR data enables us to measure the heights of the distal ramparts at 20 different locations for this Chryse crater (Fig. 10), and measure the rim crest elevation at 11 locations. In Fig. 11a we show that our inference that the rim height of the parent crater plays an important role in controlling the runout distance is not valid for the Chryse crater. Almost all of the rim heights are in the range 320–400 m, but there is considerable variability in runout distance, varying from 1.5 to 2.3 times the crater radius (i.e., 11.9–18.1 km from the rim). Despite this lack of correlation with the data for Toconao, we note that the radial extent of the ejecta for both craters, when normalized to the radius of the parent crater, are very similar with only a few of the Toconao ramparts being at greater distances than the Chryse crater. This may have significance for future studies of the effects of elevation on the mobility of the ejecta layers, as the two craters are almost equally distant from the equator.

We can also explore the comparative geometry of the ejecta blankets of the Toconao and Chryse craters using our derived data. Measurements of the difference in height between the proximal and distal base of the rampart (i.e., parameters 4 and 6 in Fig. 8) may indicate whether the ejecta layer was depositing material during the radial flow away from the rim crest. If the heights on both sides of the rampart are almost equal, this would indicate that there was little deposition of material up-range of the point where the rampart started to form. A large height difference (i.e., higher up-range than down-range) would indicate that material was deposited all the way from the rim crest to the rampart. Furthermore, we can explore the question of whether the height of the rampart is affected by the amount of material deposited within the ejecta blanket.

Figure 11b illustrates this relationship for the two craters studied here, and shows that the Chryse crater has a tendency towards a limiting thickness for the ejecta blanket up-slope of the rampart, with the maximum value being ~40 m thicker up-slope of the rampart than the surrounding land beyond the rampart. At Toconao, the proximal ejecta are only rarely thicker than 15 m on the distal side. Lower ramparts do not appear to be associated with ejecta blankets where deposition has taken place within the proximal part of the ejecta blanket. Thus the profile shown in Fig. 3 is representative of Toconao, but not the Chryse crater. Finally, we note that the negative height differences shown in Fig. 11b are the result of the ejecta coming to rest while moving up-slope.

CONCLUSIONS

The existence of ejecta around SLE and MLE craters on Mars that show evidence of surface flow, such as the diversion of ejecta by low topographic obstacles (Carr et al. 1977; Wohletz and Sheridan 1983; Baloga et al. 2005), suggests the emplacement of ejecta at slow speed (perhaps a few tens of meters per second; Baloga et al. 2005). It was probably near the final phase of ejecta emplacement that the distal ramparts were formed and that in some instances there was very little deposition prior to rampart formation. Thus important factors for the degree of fluidization of the ejecta, the size distribution of the particles that make up the final ejecta deposit, and the physical state of the target volatiles, might be contained within the structure and morphology of the ramparts. In this section we summarize our findings and propose additional research directions.

Our analysis of MOC and THEMIS images has revealed that “boulders” appear to collect at the distal margin of the ejecta, which agrees with the thermal infrared observations of Baratoux et al. (2005) that there is an increase in particle size at the margins of the ejecta blanket. These boulders may be large pieces of ejecta that were transported radially away from the ejecta within the surface flow. Alternatively, they may be more resistant erosional remnants formed in situ by a process

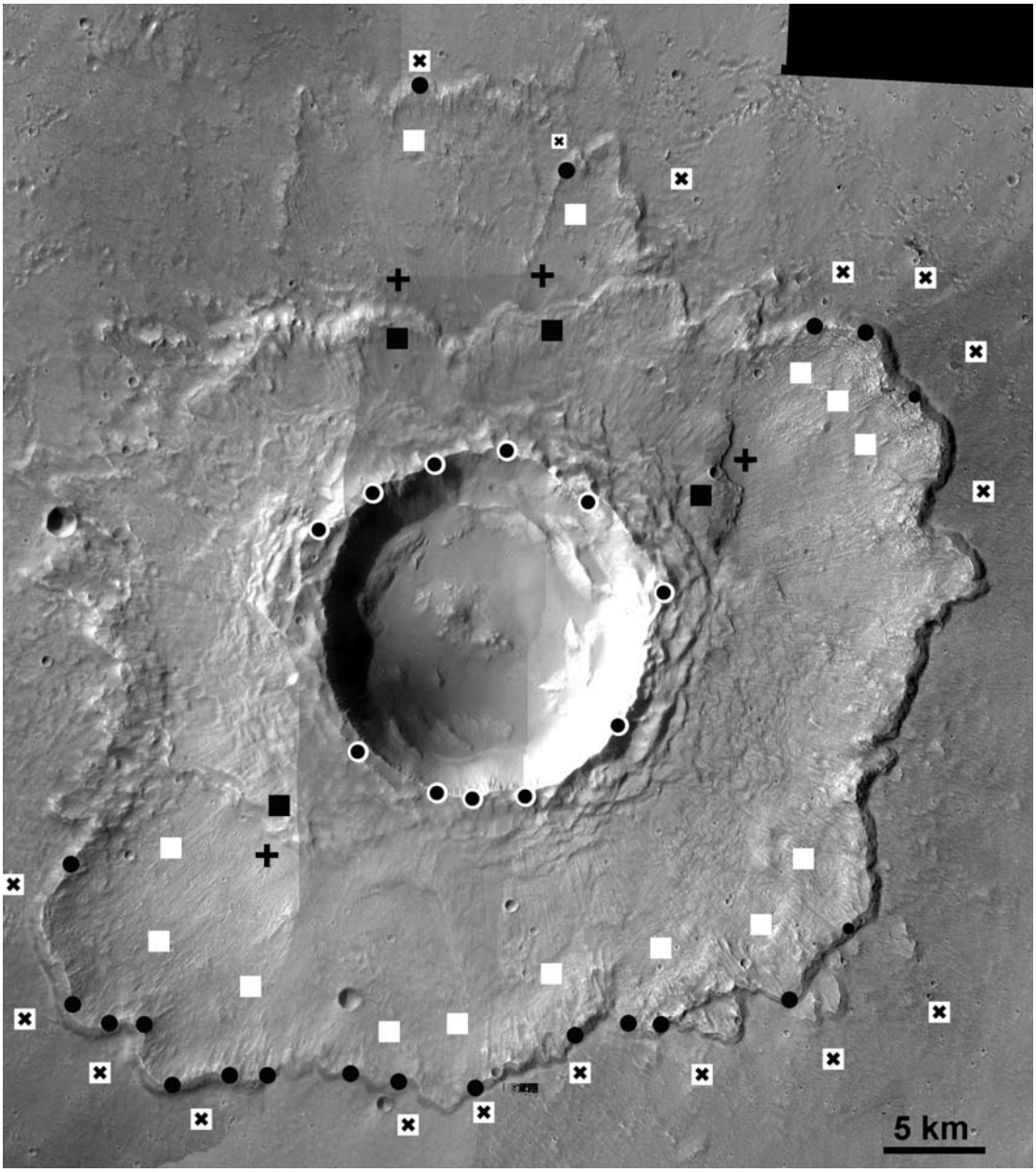

Fig. 10. A second crater, this one located in Chryse Planita (at 28.4°N, 319.4°E) has also been investigated to explore the relationships between rampart height and ejecta travel distance. The symbols used here are the same as those in Fig. 6. Mosaic of THEMIS images V04333003, V10287006, V10599013, V12446004, and V12758004.

akin to vapor phase alteration of terrestrial ignimbrites (Sheridan 1970; Fenner 1984) and are now being exposed on the surface as the ejecta is eroded. Tooting crater shows a particularly clear example of these ejecta blocks (Fig. 2b); the fact that the majority of the Tooting crater ejecta blanket appears almost unmodified by eolian erosion suggests that these blocks are of primary origin.

Ramparts are asymmetric in their cross-sectional shape (Fig. 3). There appears to be no strong correlation between the size of the rampart and the location of the parent crater on the planet. Although it is possible that greater ejecta fluidization might be associated with higher latitude (Mouginis-Mark 1979; Barlow and Perez 2003), the resultant deposit once the ejecta flow came to a standstill shows no detectable spatial difference in mechanical strength, as demonstrated by the uniform base-to-height ratio of the rampart. Indeed, the formational process by which ramparts were created remains enigmatic because we not only see ramparts at the distal edge of the ejecta deposit, but also find ramparts along on the sides of ejecta layers (Fig. 2c). These lateral ramparts, presumably, cannot be deceleration ridges akin to the distal ramparts. In addition, we see many instances of ramparts within the central

portion of the ejecta layers. This is probably significant, because it implies that there was not a single episode of ejecta flow; rather there may have been smaller, late-stage, flows within the boundaries of the ejecta layers that experienced additional deceleration events. Ramparts within the main ejecta flow typically appear to have less relief and are smaller in width and length than the distal ramparts.

Detailed analysis of the ejecta blanket of the Toconao crater reveals certain trends in the geometry of the ramparts that most likely relate to the flow process. It seems likely that the majority of the ejecta had similar properties in all radial directions in terms of particle size distribution and target volatile content because the target material appears to be uniform ridged plains materials of Sinai Planum. Thus the greater down-slope runout of ejecta where the height drop is greatest (Fig. 9) is most easily explained as the ejecta moving as a continuum flow with a significant gravity-driven influence. This further supports the longstanding concept of emplacement as a ground-hugging continuum flow. However, none of the models proposed to date explicitly considers gravity as a significant influence on the emplacement dynamics. In cases where such asymmetries can be identified and measured, this potentially provides an important new constraint on the way flow momentum is dissipated and would help in identifying the presently unknown physical processes that cause the cessation of flow advance (Barnouin-Jha et al. 2005; Baloga et al. 2005).

The lack of correlation between the height of the rampart and the radial distance from the parent crater implies that the ejecta blanket must be very thin upslope from the rampart, and that the material forming the rampart was produced from a majority of the radial ejecta flow. This interpretation is supported by our measurements of the proximal and distal heights of the terrain either side of the rampart (Fig. 11b), and the inference that the majority of the ejecta blankets that were mapped from Viking Orbiter images (Wohletz and Sheridan 1983; Barlow and Bradley 1994) now appear to be mainly thin veneers on the Martian landscape and only the familiar distal rampart allows the extent of the ejecta blanket to be identified. From Fig. 11b, we also conclude that the volume of material deposited within the distal rampart is not influenced by the proportion of ejecta deposited within the main part of the ejecta blanket.

The above uncertainties in the mode of formation of the distal ramparts, and their probable significance in the unraveling of the role of fluidization in the emplacement process, raise several questions that will need additional geomorphic data to resolve. Specifically, the high-resolution (<1 m/pixel) images that will be collected of Mars from the high-resolution topographic data to be derived from the stereo images from the High-Resolution Imaging Science Experiment (HiRISE) onboard Mars Reconnaissance Orbiter (MRO), along with the stereographically derived elevation data (at a spatial scale of a few meters) for small areas from

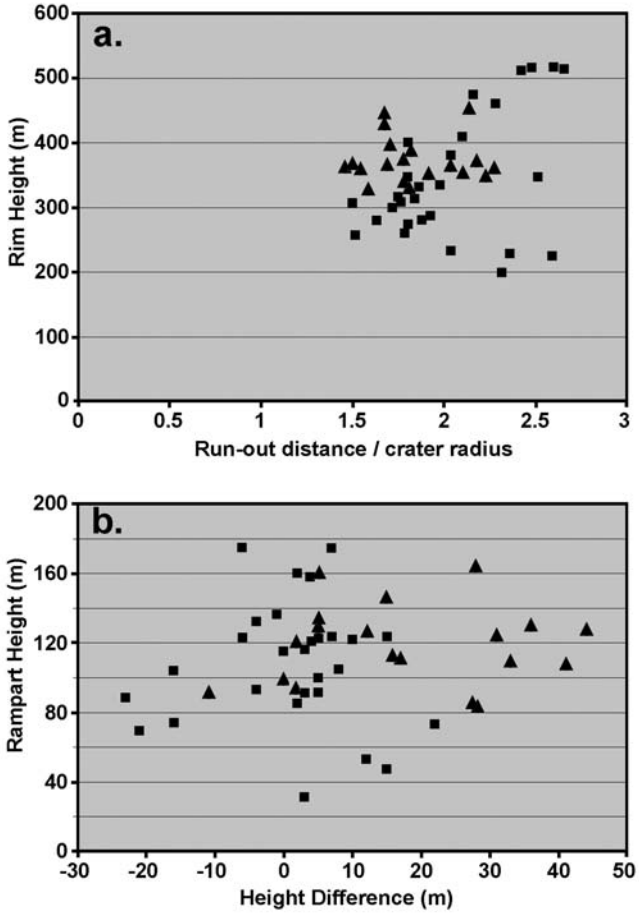

Fig. 11. A comparison of the geometry of Toconao crater and the unnamed crater in Chryse Planitia. a) Runout distance, normalized to the radius of the parent crater, compared to the rim height of the crater. Compare with Fig. 9d. b) Height difference between the elevation of the terrain beyond the rampart and the elevation of the ejecta just proximal to the rampart, compared to the rampart height. Positive numbers for the height difference signify that the ejecta is higher than the surrounding terrain. Triangles denote the Chryse crater, and the squares denote Toconao crater.

the same instrument, could be crucial in resolving spatial trends in rampart geometry that may pertain to the extent of ejecta fluidization. We believe that structures within the ramparts, such as layering in the deposit or additional evidence for size-sorting of the entrained particles in the decimeter- to meter-scale, may be visible in HiRISE images. Furthermore, unlike the widely spaced MOLA ground tracks, the stereo data from HiRISE will enable the shape (width, height, and cross-sectional profile) of many more ramparts to be confidently measured. We therefore speculate that a systematic analysis of rampart heights at different latitudes and elevations, as well as a more complete analysis of the radial variations in rampart base-to-height ratio for individual craters, may yet reveal subtle attributes of the rheology of the ejecta flows. Such studies await the return of MRO data.

Acknowledgments–This work was supported in part by NASA grant NAG5-13420 to PMM and NAG-10530 to SMB. We thank Harold Garbeil for producing the software that is used extensively in this work for merging the MOLA ground tracks with the THEMIS VIS images. Phil Christensen and the THEMIS Science Team, especially Laurel Cherednik, Kelly Bender, and Abdreas Dombovari, were responsible for the targeting of THEMIS instrument to collect the near-complete coverage of the Tooting and Toconao craters. Mike Malin and Ken Edgett are thanked for specifically targeting the MOC instrument to obtain the image used in Fig. 2d under the MOC Public Target Request Program. Nadine Barlow and Robert Herrick provided valuable reviews to an earlier version of this manuscript. This is HIGP Publication No. 1461 and SOEST Contribution No. 6963.

Editorial Handling—Dr. Nadine Barlow

REFERENCES

Baloga S. M., Fagents S. A., and Mouginis-Mark P. J. 2005. The emplacement of Martian rampart deposits. *Journal of Geophysical Research*, 110, doi:10.1029/2004JE002338.

Baratoux D., Delacourt C., and Allemand P. 2002. An instability mechanism in the formation of the Martian lobate craters and the implications to the rheology of ejecta. *Geophysical Research Letters* 29, doi:10.1029/2001GL013779.

Baratoux D., Magnold N., Pinet P., and Costard F. 2005. Thermal properties of lobate ejecta in Syrtis Major, Mars: Implications for the mechanisms of formation. *Journal of Geophysical Research* 110, doi:10.1029/2004JE002314.

Barlow N. G. 1994. Sinuosity of Martian rampart crater deposits. *Journal of Geophysical Research* 99:10,927–10,935.

Barlow N. G. 2004. Martian subsurface volatile concentrations as a function of time: Clues from layered ejecta craters. *Geophysical Research Letters* 31, doi:10.1029/2003GL019075.

Barlow N. G. 2005. A review of Martian impact crater ejecta structures and their implications for target properties. In *Large meteorite impacts III*. Boulder, Colorado: Geological Society of America. pp. 433–442.

Barlow N. G. and Bradley T. L. 1994. Martian impact craters: Correlations of ejecta and interior morphologies with diameter, latitude, and terrain. *Icarus* 87:156–179.

Barlow N. G. and Perez C. B. 2003. Martian impact crater ejecta morphologies as indicators of the distribution of subsurface volatiles. *Journal of Geophysical Research* 108, doi:10.1029/2002JE002036.

Barlow N. G., Boyce J. M., Costard F. M., Craddock R. A., Garvin J. B., Sakimoto S. E. H., Kuzmin R. O., Roddy D. J., and Soderblom L. A. 2000. Standardizing the nomenclature of Martian impact crater ejecta morphologies. *Journal of Geophysical Research* 105:26,733–26,738.

Barnouin-Jha O. S. 2005. The runout efficiency of fluidized ejecta on Mars (abstract). Workshop on the Role of Volatiles and Atmospheres on Martian Impact Craters. pp. 21–22.

Barnouin-Jha O. S. and Schultz P. H. 1998. Lobateness of impact ejecta deposits from atmospheric interactions. *Journal of Geophysical Research* 103:25,739–25,756.

Barnouin-Jha O. S., Baloga S., and Glaze L. 2005. Comparing landslides to fluidized crater ejecta on Mars. *Journal of Geophysical Research* 110, doi:10.1029/2003JE002214.

Boyce J. M. and Mouginis-Mark P. J. Forthcoming. Martian craters viewed by the THEMIS instrument: Double-layered ejecta craters. *Journal of Geophysical Research*.

Carr M. H., Crumpler L. S., Cutts J. A., Greeley R., Guest J. E., and Masursky H. 1977. Martian impact craters and emplacement of ejecta by surface flow. *Journal of Geophysical Research* 82: 4055–4065.

Costard F. M. 1989. The spatial distribution of volatiles in the Martian hydrolithosphere. *Earth, Moon, and Planets* 114:93–112.

Davis P. A. and Soderblom L. A. 1984. Modeling crater topography and albedo from monoscopic Viking Orbiter images. 1. Methodology. *Journal of Geophysical Research* 89:9449–9457.

Fenner C. N. 1984. Incandescent tuff flows in southern Peru. *Geological Society of America Bulletin* 59:879–893.

Gault D. E. and Greeley R. 1978. Exploratory experiments of impact craters formed in viscous-liquid targets: Analogs for Martian rampart craters? *Icarus* 34:486–495.

Horner V. M. and Greeley R. 1982. Pedestal craters on Ganymede. *Icarus* 51:544–562.

Horner V. M. and Greeley R. 1987. Effects of elevation and ridged plains thicknesses on Martian crater ejecta morphology. Proceedings, 17th Lunar and Planetary Science Conference. *Journal of Geophysical Research* 92:E561–E569.

Ivanov B. A. 1996. Spread of ejecta from impact craters and the possibility of estimating the volatile content of the Martian crust. *Solar System Research* 30:43–58.

Moore J. M., Asphaug E., Belton M. J. S., Bierhaus B., Breneman H. H., Brooks S. M., Chapman C. R., Chuang F. C., Collins G. C., Giese B., Greeley R., Head J. W., Kadel S., Klaasen K. P., Klemaszewski J. E., Magee K. P., Moreau J., Morrison D., Neukum G., Pappalardo R. T., Phillips C. B., Schenk P. M., Senske D. A., Sullivan R. J., Turtle E. P., and Williams K. K. 2001. Impact features on Europa: Results of the Galileo Europa Mission (GEM). *Icarus* 151:93–111.

Mouginis-Mark P. J. 1978. Morphology of Martian rampart craters. *Nature* 272: 691–694.

Mouginis-Mark P. J. 1979. Martian fluidized crater morphology: Variations with crater size, latitude, altitude, and target material. *Journal of Geophysical Research* 84:8011–8022.

Mouginis-Mark P. J. 1981. Ejecta emplacement and modes of formation of Martian fluidized ejecta craters. *Icarus* 45:60–76.

Schultz P. H. 1992. Atmospheric effects on ejecta emplacement. *Journal of Geophysical Research* 97:11,623–11,662.

Schultz P. H. and Gault D. E. 1979. Atmospheric effects on Martian ejecta emplacement. *Journal of Geophysical Research* 84:7669–7687.

Schultz P. H. and Gault D. E. 1982. Impact ejecta dynamics in an atmosphere: Experimental results and extrapolations. In *Geological implications of impacts of large asteroids and comets on the Earth*, edited by Silver L. T. and Schultz P. H. Boulder, Colorado: Geological Society of America. pp. 153–174.

Sheridan M. F. 1970. Fumarolic mounds and ridges of the Bishop tuff, California. *Geological Society of America Bulletin* 81:851–868.

Sheskin D. J. 1997. *Handbook of parametric and nonparametric statistical procedures*. New York: CRC Press.

Shreve R. L. 1968. *The Blackhawk landslide*. Boulder, Colorado: Geological Society of America. 47 p.

Wohletz K. H. and Sheridan M. F. 1983. Martian rampart crater ejecta: Experiments and analysis of melt water interaction. *Icarus* 56:15–37.